

Probing of electromagnetic fields on atomic scale by photoelectric phenomena in graphene

P. Olbrich,¹ C. Drexler,¹ L.E. Golub,² S. N. Danilov,¹ V. A. Shalygin,³
 R. Yakimova,⁴ S. Lara-Avila,⁵ S. Kubatkin,⁵ B. Redlich,⁶ R. Huber,¹ S. D. Ganichev¹
¹ *Terahertz Center, University of Regensburg, 93040 Regensburg, Germany*
² *Ioffe Physical-Technical Institute, Russian Academy of Sciences, 194021 St. Petersburg, Russia*
³ *St. Petersburg State Polytechnic University, 195251 St. Petersburg, Russia*
⁴ *Linköping University, S-58183 Linköping, Sweden*
⁵ *Chalmers University of Technology, S-41296 Göteborg, Sweden and*
⁶ *FOM Institute for Plasma Physics “Rijnhuizen”,
 P.O. Box 1207, NL-3430 BE Nieuwegein, The Netherlands*
 (Dated: September 20, 2018)

We report on the observation of the reststrahl band assisted photocurrents in epitaxial graphene on SiC excited by infrared radiation. The peculiar spectral dependence for frequencies lying within the reststrahl band of the SiC substrate provides a direct and noninvasive way to probe the electric field magnitude at atomic distances from the material’s surface. Furthermore our results reveal that nonlinear optical and optoelectronic phenomena in 2D crystals and other atomic scale structures can be giantly enhanced by a proper combination of the spectral range and substrate material.

PACS numbers: 73.50.Pz, 81.05.ue, 78.67.Wj, 42.70.Nq

Since the discovery of graphene, optical and optoelectronic properties of two dimensional (2D) crystals have attracted continuously growing attention [1]. A keen interest has been motivated by the prospective application of mono- or few-layer systems in nonlinear optics [2–6], solar cells [7], displays [8], optoelectronics [9], sensors [10, 11], or plasmonic devices [12, 13]. Bridging the size mismatch between macroscopic photonics and atomic-scale integrated electronics all these concepts universally depend on a key quantity: the local optical fields acting on the charge carriers in 2D systems. These fields deviate from the emitted or incident waves due to the dielectric environment of the supporting substrate. A mesoscopic description has been invoked to obtain electromagnetic fields in the vicinity of a fictitious effective medium characterized by a mathematically sharp interface and bulk dielectric functions [12–15]. Yet, in the extreme limit, of an atomic thin system a mesoscopic model is not justified a priori and electromagnetic fields may be altered by the modified polarization response of the surface structure.

At the same time, the precise knowledge of the local electromagnetic fields is particularly important for phenomena that scale nonlinearly with the field amplitude. Examples range from optical nonlinearities to high-frequency transport as studied in 2D crystals [2–6, 12–20], carbon nanotubes [21–24], topological insulators [25–27] and single molecules [28]. Nonetheless, measuring electric fields on atomic distances is challenging. Surface-confined plasma oscillations in graphene have shown to change their dispersion sensitively in the spectral vicinity of the reststrahl band [29] of substrates [30]. They could, thus, be basically used as sensors for the local dielectric environment. Yet, the depth resolution of the evanescent field remains on the order of several 100 nm. Even for near-field microscopy reaching extreme sub-wavelength spatial resolution [13] or a recent approach tracing the natural optical-frequency magnetic dipole transitions in lan-

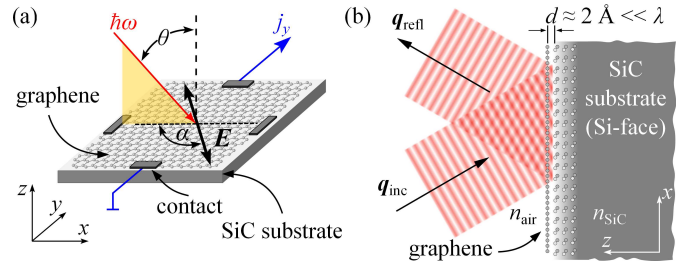


Figure 1: (a) experimental geometry (b) reflection of a plane wave from a graphene layer on a SiC substrate deposited at the distances of about 2 Å from the surface.

thanide ions [31], the atomic scale has been out of reach.

Here, we demonstrate that measurements of high frequency photoelectric effects in graphene deposited on a substrate provide a direct way to probe the electric field magnitude, E_0 , at atomic distances from the material’s surface. We show that second-order photoelectric effects excited in graphene exhibit a peculiar spectral dependence for frequencies lying within the reststrahl band of the SiC substrate. The resonances of the photocurrents are attributed to the variation of the out-of-plane and in-plane components of the radiation electric field acting on electrons that are confined in the graphene layer deposited at a distance $d \approx 2 \text{ \AA}$ from the SiC surface, see Fig. 1(b) and Ref. 32. We show that an analysis of the field distribution based on the macroscopic Fresnel formulas surprisingly well describes all experimental findings, while there remain quantitative discrepancies. As an important result, the observed reststrahl band assisted photocurrent also clearly demonstrates that nonlinear optical and optoelectronic phenomena in 2D crystals, carbon nanotubes and topological insulators can be giantly enhanced by a proper combination of the spectral range and substrate material.

Photocurrents have been observed in several large area n -type graphene monolayer samples [17, 33] at room tem-

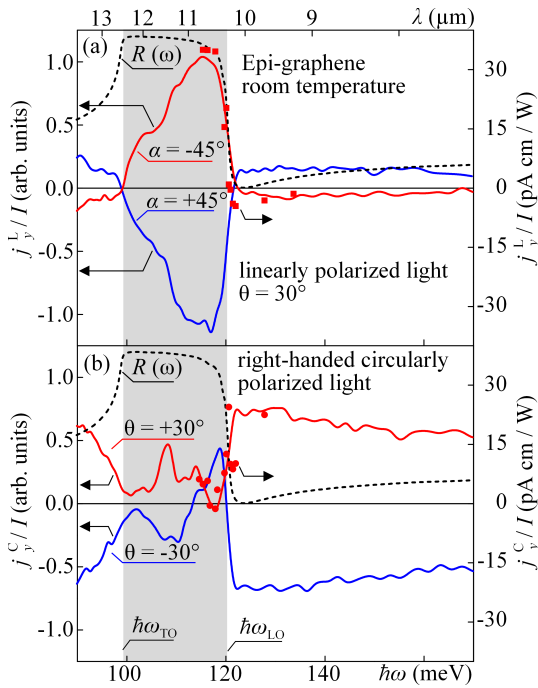


Figure 2: Spectra of the photocurrent excited by (a) linearly and (b) circularly polarized radiation. Solid lines and circles show the data obtained with free electron and cw CO₂ lasers, respectively. Dashed lines show the reflection spectra $R(\omega)$, which reveals a clear reststrahl band of SiC (gray area) with maximum reflection of about 100%.

perature. Figure 1(a) depicts the corresponding experimental geometry. To induce the photocurrents we used the radiation of the pulsed free electron laser “FELIX” operating at tunable wavelength λ from 7 to 16 μm or a cw CO₂ laser. Radiation was applied in the (xz) plane at an angle of incidence θ , varied between -30° to $+30^\circ$ to the layer normal, z . Details on the sample preparation and experiments are given in the supplementary material.

Illuminating an unbiased graphene layer with polarized radiation at oblique incidence we detected a photocurrent signal whose spectral behaviour is shown in Fig. 2. Panel (a) shows the photocurrent j_y^L excited by linearly polarized radiation with the azimuth angle $\alpha = \pm 45^\circ$ (see Fig. 1(a)). A remarkable observation is that the current in the range of photon energies $\hbar\omega$ between about 99 and 120 meV changes sign while its value increases by more than an order of magnitude compared to that excited by light with lower and higher frequencies. Despite the fact that the photocurrent shows a peculiar spectral dependence the overall functional behaviour of the photocurrent remains unchanged in the whole frequency range: The current i) scales linearly with the radiation intensity $I \propto E_0^2$ ii) is characterized by a short response time and iii) varies with the azimuthal angle α and the angle of incidence θ as $j_y^L = L \sin 2\alpha \sin \theta E_0^2$, where L is a prefactor. In particular, it reverses its direction by changing α from $+45^\circ$ to -45° for a fixed θ , see Fig. 2(a) as well as upon switching $\theta = +30^\circ$ to -30° (not shown). Studying the radiation reflection, see dashed lines in Fig. 2 and supplementary materials, reveals that the position and width of the pho-

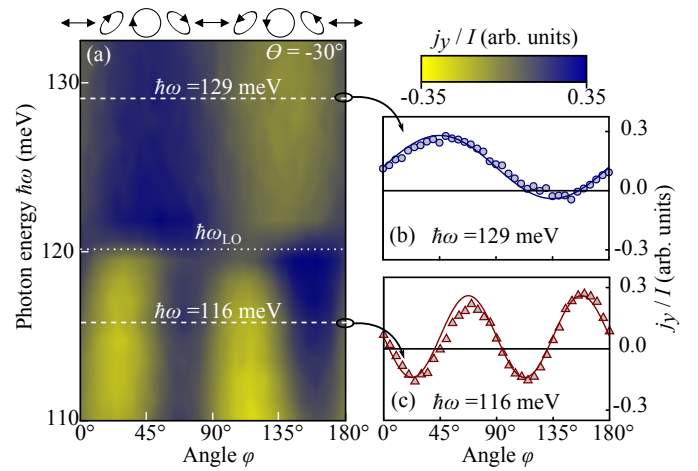


Figure 3: (a) Photocurrent j_y/I as a function of the phase angle φ defining radiation helicity and photon energy $\hbar\omega$. (b) and (c) show corresponding dependences obtained for $\hbar\omega = 129$ meV and 116 meV, respectively. The ellipses on top of the panel (a) illustrate the polarization states for several angles φ .

tocurrent resonance matches well the reststrahl band of the SiC [30, 34], which is characterized by an almost total reflection $R(\omega)$ between the longitudinal, $\hbar\omega_{\text{LO}}$, and transversal, $\hbar\omega_{\text{TO}}$, optical phonon energies.

The photocurrent is also observed for elliptically (circularly) polarized radiation, obtained via rotation of Fresnel rhombus by the angle φ . By that we controllably vary the degree of linear, $P_l = \sin 4\varphi/2$, and circular, $P_c = \sin 2\varphi$, polarization, respectively. Figure 3(a) shows the polarization dependence of j_y measured for different photon energies in the vicinity of the reststrahl band. The detected photocurrent can be well fitted by $j_y = j_y^L + j_y^C = [(L/2) \sin 4\varphi + C \sin 2\varphi] \sin \theta E_0^2$ as shown in Figure 3(b) and (c) for photon energies below and above $\hbar\omega_{\text{LO}}$, respectively. Here the linear photocurrent j_y^L , given by the fourth harmonics of φ , is just the above discussed current in response to linearly polarized radiation but excited by elliptically polarized light. By contrast, the circular current j_y^C stems from the radiation helicity and is proportional to the degree of circular polarization P_c : It achieves a maximum for circularly polarized radiation and reverses its direction by switching from right- to left-handed polarized light. Figure 3 reveals the crossover from the dominating circular ($\propto \sin 2\varphi$) to linear ($\propto \sin 4\varphi$) photocurrent contributions in the vicinity of $\hbar\omega_{\text{LO}}$. The spectral behaviour of the circular contribution, j_y^C , is shown for right-handed circular polarization in Fig. 2 (b). Similar to the linear photocurrent we found here a peculiar spectral behaviour within the reststrahl band. However, by contrast to j_y^L , the circular photocurrent is not enhanced but rather suppressed. It has a complex spectral behaviour exhibiting a change of sign and a dip close to the center of the reststrahl band. Comparing circular and linear photocurrent spectra in the whole investigated range we see that the circular photocurrent j_y^C dominates for frequencies below $\hbar\omega_{\text{TO}}$ and above $\hbar\omega_{\text{LO}}$, while the linear current j_y^L is almost vanishing outside of the reststrahl band.

The microscopic origin of the photocurrent under study outside of the reststrahl band has been previously investigated in Ref. [18]. It has been demonstrated that the current is caused by a sum of the photon drag (PDE) and photogalvanic (PGE) effects of comparable strength. In particular, it has been shown that the photon drag effect in graphene is caused by a simultaneous action of the electric and magnetic field components of the infrared radiation and, in fact, can be classified as a dynamic Hall effect [16]. The origin of the photogalvanic effect is the asymmetry of electron scattering induced by radiation and structure inversion asymmetry [18, 35]. The addressed above fact that all characteristic features of the photocurrent are the same within and outside the reststrahl band, indicates that its microscopic origin remains unchanged. Actually, this is not surprising because for normal incidence, $\hbar\omega \ll E_F$, and room temperature no resonances are expected for the light-matter interaction in pristine graphene. However, one can expect dramatic modifications of local electric fields acting on carriers in graphene for frequencies within the reststrahl band of the substrate, which is characterized by a negative dielectric constant of the material. Indeed the coincidence of the increased reflection with the observed resonance of the photocurrent clearly indicates the common origin of both effects.

As we show below, the resonant photoresponse excited in graphene by radiation with frequencies within the reststrahl band of the substrate can be well understood considering only the spectral behaviour of the in-plane and out-of-plane radiation electric field components, without going into microscopic details. The required electric field components responsible for the photocurrent formation provides the phenomenological theory of PDE and PGE. In line with the experiment we consider the transverse photocurrent j_y generated in the direction perpendicular to the incidence plane (xz). Following Ref. 6 the current density due to the photon drag effect is given by

$$j_y^{PDE} = Tq_x(E_x E_y^* + E_x^* E_y) + T'q_x i(E_y E_x^* - E_x E_y^*), \quad (1)$$

and due to the photogalvanic effect by

$$j_y^{PGE} = \chi(E_z E_y^* + E_y E_z^*) + \gamma i(E_z E_y^* - E_y E_z^*). \quad (2)$$

Here E is the electric field acting on electrons, T and χ are coefficients describing, respectively, the PDE and PGE [36] currents proportional to the linear polarization degree P_l given by symmetrical combinations of electric field components. The two remaining coefficients correspond to the circular PDE (T') and PGE (γ) currents. These contributions reverse the direction upon switching the photon helicity $P_c = i(\mathbf{E} \times \mathbf{E}^*) \cdot \mathbf{q}/q$.

In the following analysis we assume coefficients χ , γ , T and T' to be frequency independent in the narrow frequency range of the reststrahl band and focus on the frequency behaviour of the electric field components only. This assumption is reasonable for the considered experimental conditions because for room temperature, $\hbar\omega \ll E_F$, and $\omega\tau \sim 1$, the radiation absorption is caused by Drude-like indirect intraband optical transi-

tions. Hence, χ , γ , T and T' have smooth frequency dependences [16, 18]. Moreover, we disregard a possible influence of graphene itself on the electric field magnitudes.

To obtain the frequency dependence of the required electric field components we use macroscopic Fresnel formulas, which, strictly speaking, are applicable for representation of dielectric medium by a homogeneous function $\varepsilon(\omega)$, which is independent of the position within the medium. In this approach the electric fields are formed by superposition of the incident and reflected waves, see Fig. 1(b). They are described by the corresponding Fresnel transmission coefficients, and, consequently, reflect the spectral behaviour of the dielectric function of the substrate, $\varepsilon(\omega)$. As it is well known, the latter exhibits a strong anomaly within the reststrahl band [29]

$$\varepsilon(\omega) = \varepsilon_\infty + \frac{\varepsilon_0 - \varepsilon_\infty}{1 - (\omega/\omega_{TO})^2 - i\omega\Gamma/\omega_{TO}^2}, \quad (3)$$

where ω_{TO} and Γ are the frequency and the damping of the TO phonon, ε_0 and ε_∞ are the low- and high-frequency dielectric constants, respectively. These dielectric constants relate ω_{TO} with the LO phonon frequency via the Lyddane-Sachs-Teller relationship, $\omega_{LO} = \sqrt{\varepsilon_0/\varepsilon_\infty}\omega_{TO}$. The complex dielectric function and, consequently, the complex refractive index $\sqrt{\varepsilon} = n + i\kappa$, determine the frequency dependence of the electric field components. Here n is refractive index and κ the extinction coefficient, see supplementary materials. The in-plane components E_x and E_y are continuous and found from the Maxwell equation $\text{div}\mathbf{E} = 0$ yielding:

$$E_x = t_p E_{0p}(n + i\kappa)\Xi, \quad E_y = t_s E_{0s}, \quad (4)$$

where E_{0s} , E_{0p} are the corresponding parts of the incident wave amplitude, $\Xi = 1/\sqrt{n^2 + \kappa^2 + \sin^2\theta_0}$, and t_s , t_p are the standard Fresnel amplitude transmission coefficients for s - and p -polarizations, see supplementary materials.

While the in-plane field components are continuous at the air/SiC interface, its normal component E_z is discontinuous having different values inside and outside the substrate given by:

$$E_z^{in} = -t_p E_{0p} \sin\theta_0 \Xi, \quad E_z^{out} = \varepsilon E_z^{in}. \quad (5)$$

Substituting the above components of the radiation electric field in Eqs. (1) and (2) we obtain spectral behaviour of the photon drag and photogalvanic currents, respectively. We start with the PDE current given by the in-plane components $E_{x,y}$ and photon wavevector $q_x = (\omega/c)\sin\theta_0$. All these quantities are continuous, therefore, from Eqs. (1) and (4) we obtain one solution for each, linear and circular, photocurrents:

$$j_y^L = \frac{\omega}{c} \sin\theta_0 P_l |E_0|^2 \times [(nT + \kappa T') \text{Re}(t_p^* t_s) + (\kappa T - nT') \text{Im}(t_p^* t_s)] \Xi, \quad (6)$$

$$j_y^C = \frac{\omega}{c} \sin\theta_0 P_c |E_0|^2 \times [(\kappa T - nT') \text{Re}(t_p^* t_s) - (nT + \kappa T') \text{Im}(t_p^* t_s)] \Xi. \quad (7)$$

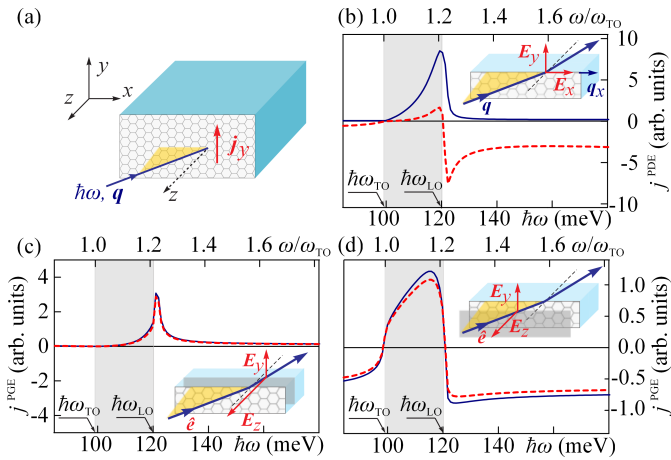


Figure 4: (a) Geometry of the photocurrent generation. (b)-(d) Calculated spectral dependence of the linear (solid) and circular (dashed) photocurrents. (b) Photon drag effect. (c) and (d) Photogalvanic effect caused by the electric field in the SiC side, \mathbf{E}^{in} , and in the air side of the air/SiC interface, \mathbf{E}^{out} , respectively. The calculations are performed for $\theta_0 = 30^\circ$, $\gamma/\chi = 0.9$, $T'/T = 18$, the damping constant $\Gamma = 0.01\omega_{TO}$ obtained from the reflection data, see Fig. 2, and SiC high- and low-frequency dielectric constants $\varepsilon_\infty = 6.52$, $\varepsilon_0 = 9.66$, respectively (see Ref. [34]). The insets show components of the electric field and photon wave vector considered in the corresponding calculations.

The above equations yield at first glance a surprising result. By contrast to Eqs. (1) the obtained linear and circular PDE currents are determined by both T and T' coefficients. This comes from the fact that, within the reststrahl band, the radiation acting on the electrons in the graphene layer becomes elliptically polarized even for irradiation with purely linear or circular light [37]. Outside the reststrahl band \Re and $\text{Im}(t_p^*t_s)$ are almost zero. Thus the linear and circular PDE currents are given solely by the coefficients T and T' , respectively.

Figure 4 (b) shows the calculated spectra of the linear and circular photon drag effect. Calculations are carried out for the dominating contribution of the circular PDE - the fact which clearly follows from the data outside the reststrahl band. Within the reststrahl band the situation changes. Due to the polarization transformation addressed above, the T' -contribution gives rise to the enhancement of the linear PDE. At the same time the decrease of the radiation helicity results in suppression of the circular photocurrent. While our calculations of the photon drag effect confirm the enhancement/suppression of the linear/circular photocurrent within the reststrahl band they do not describe the double sign inversion and significant value of the linear photocurrent detected outside the reststrahl band, see Fig. 4 (a).

To obtain a better agreement we consider the photogalvanic effect which, according to Ref. [18], should yield a comparable contribution to the total photocurrent excited by infrared radiation. It follows from Eqs. (2) that all PGE contributions require a normal component of the electric field, which is discontinuous at the interface. Therefore, from Eqs. (2) and (5) we obtain different solu-

tions for the photocurrents excited by the field in the air side of the air/SiC interface, E_z^{out} :

$$j_y^L = -\sin\theta_0 P_1 |E_0|^2 [\chi \text{Re}(t_p^* t_s) + \gamma \text{Im}(t_p^* t_s)] \Xi, \quad (8)$$

$$j_y^C = -\sin\theta_0 P_c |E_0|^2 [\gamma \text{Re}(t_p^* t_s) + \chi \text{Im}(t_p^* t_s)] \Xi, \quad (9)$$

and from the field in the SiC side of the interface, E_z^{in} :

$$j_y^L = -\sin\theta_0 P_1 |E_0|^2 [\chi \text{Re}(t_p^* \varepsilon^* t_s) + \gamma \text{Im}(t_p^* \varepsilon^* t_s)] \Xi, \quad (10)$$

$$j_y^C = -\sin\theta_0 P_c |E_0|^2 [\gamma \text{Re}(t_p^* \varepsilon^* t_s) + \chi \text{Im}(t_p^* \varepsilon^* t_s)] \Xi. \quad (11)$$

The resulting calculations, applying the same parameters as that used for calculations of PDE, are shown in Figs. 4 (c), (d). It is seen that both linear and circular photogalvanic currents show a strong enhancement in the reststrahl band. The solutions for the electric field in the substrate, see Fig. 4 (c), yield a sharp peak close to the longitudinal optical phonon energy only and, thus, do not describe the complex spectral behaviour of the photocurrent shown in Fig. 5 (a). Moreover, we did not detect any sharp peak at LO frequency, which supports the conclusion that this contribution to the total photocurrent is negligible. A good agreement with the experiment is obtained for the linear photogalvanic current excited by the electric field in the air side of the air/SiC interface, see Fig. 4 (d). However, this solution does not describe the suppression of the circular photocurrent. We emphasize, that this disagreement can not be avoided simply by variation of the ratio between the coefficients γ and χ describing the linear and circular photogalvanic currents, respectively.

Our calculations show that the overall reasonable agreement can only be achieved by considering a superposition of both PDE and PGE photocurrents. The corresponding results together with experimental data are shown in Fig. 5. In fact, the calculations reflect all main features of the measured photocurrent, namely: i) Both circular and linear currents depend weakly on the frequency outside the reststrahl band; ii) The linear current changes its sign and has a broad peak within the whole reststrahl band; iii) The circular current is suppressed and has an asymmetric double-peak structure; iv) The linear current dominates the circular one within the reststrahl band and vice versa in the outside. We emphasize that, a satisfying agreement is obtained despite the fact that the calculations are carried out for the homogeneous functions $\varepsilon(\omega)$, abrupt interfaces and the influence of graphene on the radiation field was disregarded. These simplifications used in our model or possible E_z -electric field induced charge transfer between graphene and SiC [38] may be responsible for remaining small discrepancies, like a more pronounced dip in the circular current close to the center of reststrahl band. A comparison of the photon drag and photogalvanic current components reveals that within the resonance the photon drag effect strongly dominates in the total current whereas outside the resonance the main contribution comes from the linear photogalvanic effect.

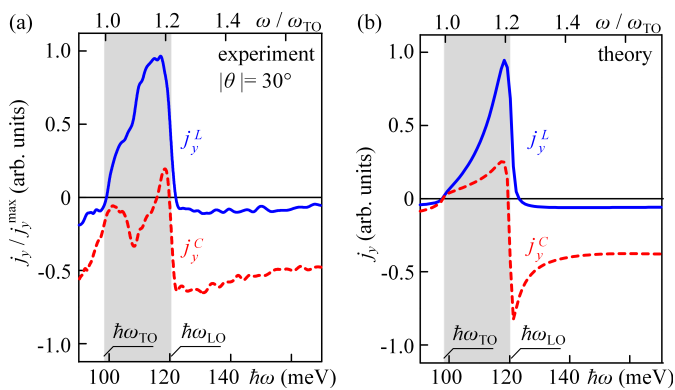


Figure 5: Spectral behaviour of the linear (solid lines) and circular (dashed lines) photocurrents. (a) Experimental results. (b) Calculated photocurrent for electric field components E_x, E_y, E_z^{out} , a ratio of PDE to PGE equal to $(\omega_{TO}/c)T'/\chi = 0.3$ and the parameters given in the caption of Fig. 4.

As for the circular photocurrent the PDE is responsible for the photoresponse in the whole studied spectral range.

To conclude, our results demonstrate that photocurrents in graphene deposited on a medium with a negative dielectric constant can be efficiently used for studies of how an electric field acts on the atomic scale. While the described approach is limited to the spectral range defined by the reststrahl band of the substrate material, radiation of any desired frequency can be analyzed using negative dielectric constant of artificially made periodic structures, like metamaterials [39]. Last but not at least, our findings demonstrate that optical and optoelectronic phenomena can be giantly enhanced in strictly two-dimensional systems and other nanoscale systems if these structures are deposited on a substrate with a negative dielectric function. This result is of importance for various kinds of applications in particularly those making use of effects proportional to higher orders of the electric field.

We thank S.A. Tarasenko and M.M. Voronov for helpful discussions. Support from DFG (SPP 1459 and GRK 1570), Linkage Grant of IB of BMBF at DLR, RFBR, and POLAPHEN is acknowledged.

[1] K. S. Novoselov *et al.*, Nature **490**, 192 (2012).
 [2] J. J. Dean and H. M. van Driel, Appl. Phys. Lett. **95**, 261910 (2009).
 [3] E. Hendry *et al.*, Phys. Rev. Lett. **105**, 097401 (2010).
 [4] M. Dragoman *et al.*, Appl. Phys. Lett. **97**, 093101 (2010).

[5] G. Hotopan *et al.*, Progress in Electromagnetic Research **118**, 57 (2011).
 [6] M. M. Glazov and S. D. Ganichev, arXiv:1306.2049v1 (2013).
 [7] K. J. Tielrooij *et al.*, Nature Phys. **9**, 248 (2013).
 [8] S. Bae *et al.*, Nature Nanotech. **5**, 574 (2010).
 [9] T. Gu *et al.*, Nature Photon., **6**, 554 (2012).
 [10] L. Vicarelli *et al.*, Nature Mater. **11**, 865 (2012).
 [11] N. L. Rangel *et al.*, J. Phys. Chem. C **115**, 12128 (2011).
 [12] J. Chen *et al.*, Nature **487**, 77 (2012).
 [13] Z. Fei *et al.*, Nature **487**, 82 (2012).
 [14] M. Jablan, H. Buljan, and M. Soljacic, Phys. Rev. B **80**, 245435 (2009).
 [15] F. H. L. Koppens, D. E. Chang, and F. J. G. de Abajo, Nano Lett. **11**, 3370 (2011).
 [16] J. Karch *et al.*, Phys. Rev. Lett. **105**, 227402 (2010).
 [17] J. Karch *et al.*, Phys. Rev. Lett. **107**, 276601 (2011).
 [18] C. Jiang *et al.*, Phys. Rev. B **84**, 125429 (2011).
 [19] D. Sun *et al.*, Phys. Rev. B **85**, 165427 (2012).
 [20] L. Prechtel *et al.*, Nature Comm. **3** 646, (2012).
 [21] A. Jorio, G. Dresselhaus, M. S. Dresselhaus, eds. in *Advanced Topics in the Synthesis, Structure, Properties and Applications*, (Springer, 2008).
 [22] E. L. Ivchenko and B. Spivak, Phys. Rev. B **66**, 155404 (2002).
 [23] G. Y. Slepyan *et al.*, Phys. Rev. A **63**, 053808 (2001).
 [24] G. M. Mikheev *et al.*, Nano Letters **12**, 77 (2012).
 [25] X.-L. Qi, S. C. Zhang, and X. L. Qi, Rev. Mod. Phys. **83**, 1057 (2011).
 [26] P. Hosur, Phys. Rev. B **83**, 035309 (2011).
 [27] J. W. McIver *et al.*, Nature Nanotech. **7**, 96 (2012).
 [28] J. Lupton, Adv. Mater. **22**, 1689 (2010).
 [29] P. Y. Yu and M. Cardona, *Fundamentals of Semiconductors: Physics and Materials Properties*, (Springer, 4th ed., 2010).
 [30] B. K. Daas *et al.*, J. Appl. Phys. **110**, 113114 (2011).
 [31] T. H. Taminiau *et al.*, Nature Comm. **3**, 979 (2012).
 [32] J. Borysiuk *et al.*, J. Appl. Phys. **105**, 023503 (2009).
 [33] C. Drexler *et al.*, Nature Nanotech. **8** 104 (2013).
 [34] L. Patrick and W.J. Chouke, Phys. Rev. B **2**, 2255 (1970).
 [35] S. D. Ganichev, E. L. Ivchenko, and W. Prettl, Physica E **14**, 166 (2002).
 [36] Note that the PGE current, being forbidden by symmetry in pristine graphene, is allowed in graphene layer on a substrate due to broken $z \rightarrow -z$ symmetry (point group C_{6v}). The samples under study are characterized by a strong structure inversion asymmetry as demonstrated in Ref. [33].
 [37] The polarization transformation is caused by existence of the imaginary parts of transmission coefficients t_p and t_s within the reststrahl band.
 [38] S. Kopylov, A. Tzalenchuk, S. Kubatkin, and V.I. Fal'ko, Appl. Phys. Lett. **97**, 112109 (2010).
 [39] L. Solymar and E. Shamonina, *Waves in Metamaterials* (Oxford Univ Press 2009).

Supplementary material for "Probing of electromagnetic field on atomic scale by photoelectric phenomena in graphene"

P. Olbrich,¹ C. Drexler,¹ L. E. Golub,² S. N. Danilov,¹ V. A. Shalygin,³
R. Yakimova,⁴ S. Lara-Avila,⁵ S. Kubatkin,⁵ B. Redlich,⁶ R. Huber,¹ S. D. Ganichev¹
¹ *Terahertz Center, University of Regensburg, 93040 Regensburg, Germany*
² *Ioffe Physical-Technical Institute, Russian Academy of Sciences, 194021 St. Petersburg, Russia*
³ *St. Petersburg State Polytechnic University, 195251 St. Petersburg, Russia*
⁴ *Linköping University, S-58183 Linköping, Sweden*
⁵ *Chalmers University of Technology, S-41296 Göteborg, Sweden and*
⁶ *FOM Institute for Plasma Physics "Rijnhuizen",
P.O. Box 1207, NL-3430 BE Nieuwegein, The Netherlands*
(Dated: September 20, 2018)

PACS numbers:

SAMPLE PREPARATION

Several large area graphene monolayer samples were grown on the Si-terminated face of a 4H-SiC(0001) semi-insulating substrate [1, 2] at $T = 2000$ °C and 1 atm argon gas pressure [6]. The layers are n -doped due to the charge transfer from SiC with a measured electron concentration in the range of 1.5×10^{12} to 7×10^{12} cm⁻², Fermi energy E_F ranging from 160 to 300 meV and mobility of about 10^3 cm²/Vs at room temperature [2–4]. The samples are characterized by a strong structure inversion asymmetry as demonstrated by the study of the magnetic quantum ratchet effect [5]. Squares with dimensions of 5×5 mm² were patterned on graphene using standard electron beam (e-beam) lithography and oxygen plasma etching. Four metallic contacts on the periphery of graphene were produced by straightforward deposition of Ti/Au (3/100 nm) through a lithographically defined mask, followed by lift-off. Ohmic contacts have been prepared at the center of the edges, with a resistance of about 2 k Ω between opposed contacts.

EXPERIMENTAL

The photocurrents were induced applying mid-infrared radiation of the frequency tunable free electron laser "FELIX" at FOM-Rijnhuizen in the Netherlands. [7] The laser operated in the spectral range between 7 μ m and 15 μ m (corresponding to photon energies from $\hbar\omega \approx 180$ meV to 90 meV). The output pulses of light from FELIX were chosen to be ≈ 2 ps long with peak power $P \approx 150$ kW, separated by 1 ns, in a train (or "macropulse") of 5 μ s duration. The beam has an almost Gaussian beam profile with a spot diameter of about 1 mm, which is measured by a pyroelectric camera [8]. The laser spot was always smaller than the sample size allowing us to avoid illumination of contacts or sample edges and, consequently, to study only photocurrents generated in pristine graphene [3]. The radiation intensity I and electric field E on the sample during the micropulse were about 20 MW/cm² and 120 kV/cm, respectively. The macropulses had a repetition rate of 10 Hz. The room

temperature photoresponse was studied in the directions perpendicular and parallel to the light incidence plane. The signals generated in the unbiased devices were measured via an amplifier with 20 MHz bandwidth and recorded with a storage oscilloscope. These measurements provide the full information about functional behaviour of the photocurrent, however, the evaluation of the current magnitude in response to such short pulses is not straightforward. Thus, to calibrate the photocurrent response we additionally measured the current excited by radiation of a line-tunable cw CO₂ laser with power P of about 40 mW. Though operating in a narrower spectral range (from 9.2 to 10.8 μ m) it provides radiation in the vicinity of the upper limit of the reststrahl band and, therefore, is appropriated for the determination of the photocurrent value in the spectral region under study. The radiation power was controlled by a photon drag detector [9] and/or a mercury cadmium teluride detector.

REFLECTION SPECTRA

Figure 1 shows the reflection spectra of graphene and SiC samples. In both samples we observed almost total reflection $R(\omega)$ between the longitudinal, $\hbar\omega_{LO}$, and transversal, $\hbar\omega_{TO}$, optical phonon energies of SiC. It is seen that reflection spectra of graphene layer on SiC slightly deviates from that of the pure SiC substrate (see dotted line in Fig. 1). This result is in agreement with the data of Ref. [10] and is attributed to the substrate phonon-induced surface plasmon-polariton formation in epitaxial graphene.

LONGITUDINAL PHOTOCURRENT

Besides the transversal photocurrent discussed in the paper, linearly polarized radiation also excites a current flowing along the light propagation direction, which varies as $j_x^L = L \cos 2\alpha \sin \theta E_0^2$ (not shown). The spectral dependence of the latter photocurrent is shown in Fig. 2 exhibiting resonance-like behaviour similar to the transversal one. For circularly polarized light the longitudinal

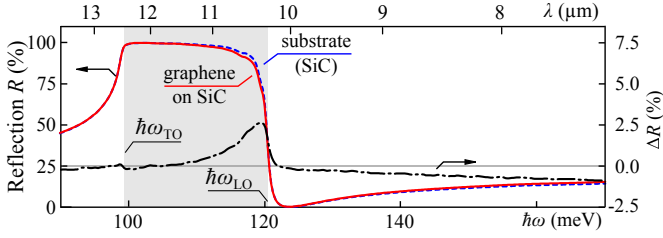


Figure 1: Dashed and solid lines show the reflection spectra of graphene on SiC substrate and pure SiC, respectively. Dotted line shows the difference between the two curves. The spectra are measured with Fourier spectrometer. Grey area shows the range of the reststrahl band of SiC limited by the energies of transverse and longitudinal optical phonons.

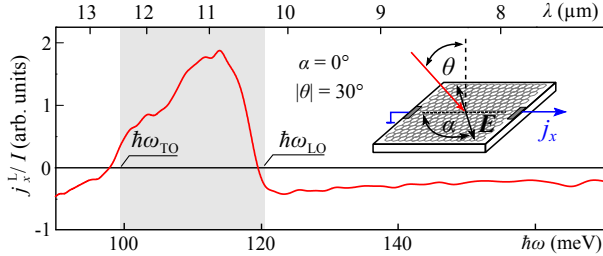


Figure 2: Spectra of the longitudinal photocurrent j_x^L measured for $|\theta| = 30^\circ$ and the azimuth angle $\alpha = 0^\circ$. The data are obtained applying linearly polarized radiation of the free electron laser "FELIX". Grey area indicates the range of the reststrahl band of SiC. The inset shows the experimental geometry.

photocurrent is not detected. The overall functional behaviour of the longitudinal photocurrent is in agreement with the phenomenological theory and microscopic picture of the photon drag and photogalvanic effects [2, 4]. Calculations of the longitudinal photocurrent applying the same set of parameters as that used in the paper are in a good agreement with the experiment.

FRESNEL TRANSMISSION COEFFICIENTS

To obtain the frequency dependence of the required electric field components we use macroscopic Fresnel formulas. They are described by the corresponding Fresnel transmission coefficients which for oblique incident radiation are given by

$$t_s = \frac{2 \cos \theta_0}{\sqrt{\varepsilon - \sin^2 \theta_0} + \cos \theta_0}, \quad (1)$$

$$t_p = \frac{2\sqrt{\varepsilon} \cos \theta_0}{\sqrt{\varepsilon - \sin^2 \theta_0} + \varepsilon \cos \theta_0}. \quad (2)$$

Consequently, electric field components reflect the spectral behaviour of the dielectric function of the substrate which is given by [11]

$$\varepsilon(\omega) = \varepsilon_\infty + \frac{\varepsilon_0 - \varepsilon_\infty}{1 - (\omega/\omega_{TO})^2 - i\omega\Gamma/\omega_{TO}^2}. \quad (3)$$

At an oblique incidence of radiation on the dielectric media with $\varepsilon(\omega)$ the wavevector component in the surface plane is $q_x = (\omega/c) \sin \theta_0$ is continuous while the normal wavevector component inside the medium $q_z^{in} = (\omega/c)(n + i\kappa)$ where [12]

$$n = \sqrt{\frac{\sqrt{(\varepsilon' - \sin^2 \theta_0)^2 + \varepsilon''^2} + \varepsilon' - \sin^2 \theta_0}{2}}, \quad (4)$$

$$\kappa = \sqrt{\frac{\sqrt{(\varepsilon' - \sin^2 \theta_0)^2 + \varepsilon''^2} - (\varepsilon' - \sin^2 \theta_0)}{2}}. \quad (5)$$

Here ε' and ε'' are the real and imaginary parts of the dielectric function (3), respectively.

-
- [1] Tzalenchuk, A. *et al.* Nature Nanotech. **5**, 186-189 (2010).
 - [2] Karch, J. *et al.* Phys. Rev. Lett. **97**, 227402 (2010).
 - [3] Karch, J. *et al.* Phys. Rev. Lett. **107**, 276601 (2011).
 - [4] C. Jiang *et al.*, Phys. Rev. B **84**, 125429 (2011).
 - [5] C. Drexler *et al.*, Nature Nanotech. **8** 104 (2013).
 - [6] K. V. Emtsev *et al.*, Nature Mat. **8**, 203 (2009).
 - [7] G. M. H. Knippels *et al.*, Phys. Rev. Lett. **83**, 1578 (1999).
 - [8] E. Ziemann *et al.*, J. Appl. Phys. **87**, 3843 (2000).
 - [9] S. D. Ganichev, Ya. V. Terent'ev, and I. D. Yaroshetskii, Pis'ma Zh. Tekh. Fiz **11**, 46 (1985) [Sov. Tech. Phys. Lett. **11**, 20 (1985)].
 - [10] B. K. Daas *et al.*, J. Appl. Phys. **110**, 113114 (2011).
 - [11] P. Y. Yu and M. Cardona, *Fundamentals of Semiconductors: Physics and Materials Properties*, (Springer, 4th ed., 2010).
 - [12] L.D. Landau and E.M. Lifshits, *Course of theoretical physics*, Vol. 8: *Electrodynamics of Continuous Media* (Pergamon, Oxford, 1984).